Supporting Information

Ge et al. 10.1073/pnas.1203743109

SI Text

Cyclic Voltammetry Simulations. The cyclic voltammograms simulated were obtained by using Digisim 3.03 assuming the following set of reactions:

$$\mathrm{A} + e^- \rightarrow \mathrm{B} \qquad \textbf{[S1]}$$

$$\mathrm{A} + \mathrm{A} \underset{k_{b1}}{\overset{k_{f1}}{\leftrightarrow}} \mathrm{C} \qquad K \qquad \textbf{[S2]}$$

$$\mathrm{C} + e^- \xrightarrow{k_{f2}} \mathrm{A} + \mathrm{B} \qquad \textbf{[S3]}$$

$$\mathrm{C} + 2e^- \rightarrow 2\mathrm{A}. \qquad \textbf{[S4]}$$

Here, A, B, C, and D represent osmocene (Cp_2Os), $[Cp_2Os^{III}]^+$, $[Cp_2Os^{III}\text{-}Os^{III}Cp_2]^{2+}$ and the reduced product of the dimer, which could be osmocene. The reaction **[S2]** proceeds with the equilibrium constant K of 2,000 and reaction **[S3]** with $k_{f2} = 0.065$.

^{1}H NMR Measurements of Osmocenium Metal-Metal Dimer Reactivity with Water. The new signal at 6.61 ppm was apparently one intermediate because it kept reacting in dark until its completion. Three other signals, one at 6.14 ppm (Product I) and the other two at 6.02 and 5.56 ppm (Product II), the intensities of which even increased in dark seemed to convert from the highly reactive intermediate ($\delta = 6.61$ ppm). Further photolysis (Fig. S6), the three peaks disappeared, faster in the signal at 6.14 ppm and slower in 6.02 and 5.56 ppm (Fig. S6). The signals at 6.02 and 5.56 seem to belong to the same complex due to their similar behavior in photolysis.

Density Functional Theory (DFT) Computations on O_2 Reduction by Osmocene. The reaction pathway computed for the reduction of oxygen by osmocene starts by formation of an oxygen-sandwich dimer $[Cp_2Os^{II}\text{-}O_2\text{-}Os^{II}Cp_2]$ with an energy of −6 (−4) kcal/mol at the B3LYP-dDsC (M06L) level. Note that the complex does not bind at B3LYP level due to the missing weak interactions between oxygen and the two osmocenium units,

$$2Cp_2Os^{II} + O_2 \rightarrow [Cp_2Os^{II}\text{-}O_2\text{-}Os^{II}Cp_2]. \qquad \textbf{[S5]}$$

In the next step this dimer complex is protonated according to reaction **[S6]**:

$$[Cp_2Os^{II}\text{-}O_2\text{-}Os^{II}Cp_2] + H_3O^+ \\ \rightarrow [Cp_2Os^{IV}(H^-)\text{-}O_2\text{-}Os^{II}Cp_2]^+ + H_2O. \qquad \textbf{[S6]}$$

At the B3LYP-dDsC and M06L levels, the protonation of the metal is 10 and 12 kcal/mol (in 1,2-DCE) more favorable than the direct formation of $HO_2\cdot$. The reaction mechanism is presented in Fig. S8 and is characterized by a reaction barrier of only 11 kcal/mol at B3LYP-dDsC and M06L levels followed by the formation of $[Cp_2Os^{III}\text{-}HO_2\text{-}Os^{II}Cp_2]^+$. Note that reaction mechanism involving protonation of one osmocene to form $[Cp_2Os^{IV}(H^-)]^+$ that then reacts with O_2 through a diradical triplet TS has a much higher barrier of 27 kcal/mol. The formation of H_2O_2 arises from the direct protonation of the hydrogen peroxyl radical, which is 14 kcal/mol more favorable than protonating the second Cp_2Os^{II} unit,

$$[Cp_2Os^{III}\text{-}HO_2\cdot\text{-}Os^{II}Cp_2]^+ + H_3O^+ \\ \rightarrow [Cp_2Os^{III}\text{-}H_2O_2\text{-}Os^{III}Cp_2]^{2+} + H_2O. \qquad \textbf{[S7]}$$

Reaction **[S7]** is exothermic (−15 kcal/mol) at B3LYP-dDsC in 1,2-DCE. Without the dDsC dispersion correction, the complex $[Cp_2Os^{III}\text{-}H_2O_2\text{-}Os^{III}Cp_2]^{2+}$ is not a stationary point on the potential energy surface. In the final step, H_2O_2 is released from the sandwiched structure $[Cp_2Os^{III}\text{-}H_2O_2\text{-}Os^{III}Cp_2]^{2+}$ and **[S8]** is energetically favored process (−8 (−14) kcal/mol at the B3LYP-dDsC (M06L) level in 1,2-DCE),

$$[Cp_2Os^{III}\text{-}H_2O_2\text{-}Os^{III}Cp_2]^{2+} \rightarrow [Cp_2Os^{III}\text{-}Os^{III}Cp_2]^{2+} + H_2O_2. \qquad \textbf{[S8]}$$

Overall, the reduction of oxygen by osmocene can be written as

$$2Cp_2Os^{II} + O_2 + 2H^+ \rightarrow [Cp_2Os^{III}\text{-}Os^{III}Cp_2]^{2+} + H_2O_2. \qquad \textbf{[S9]}$$

The reaction is highly exothermic (−42 and −38 kcal/mol at B3LYP-dDsC and M06L, respectively).

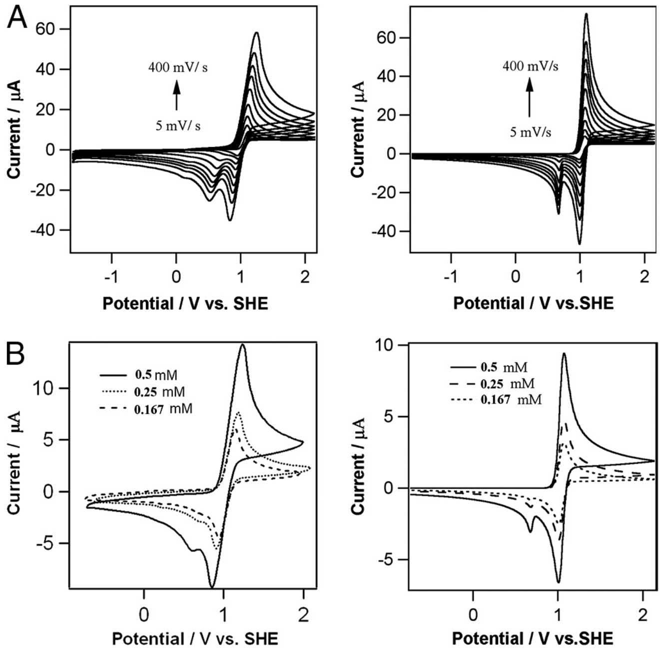

Fig. S1. Cyclic voltammetry of 2 mM Cp_2Os in 1,2-dichloroethane (1,2-DCE) on a glassy carbon electrode in anaerobic conditions. Supporting electrolyte: 25 mM bis(triphenylphosphoranylidene)-ammonium tetrakis-(pentafluorophenyl)borate (BATB) (*Left*) experimental values (*Right*) digisim simulations. (*A*) Scan rate dependence: 5 to 400 $mV \cdot s^{-1}$, (*B*) Cp_2Os concentration dependence.

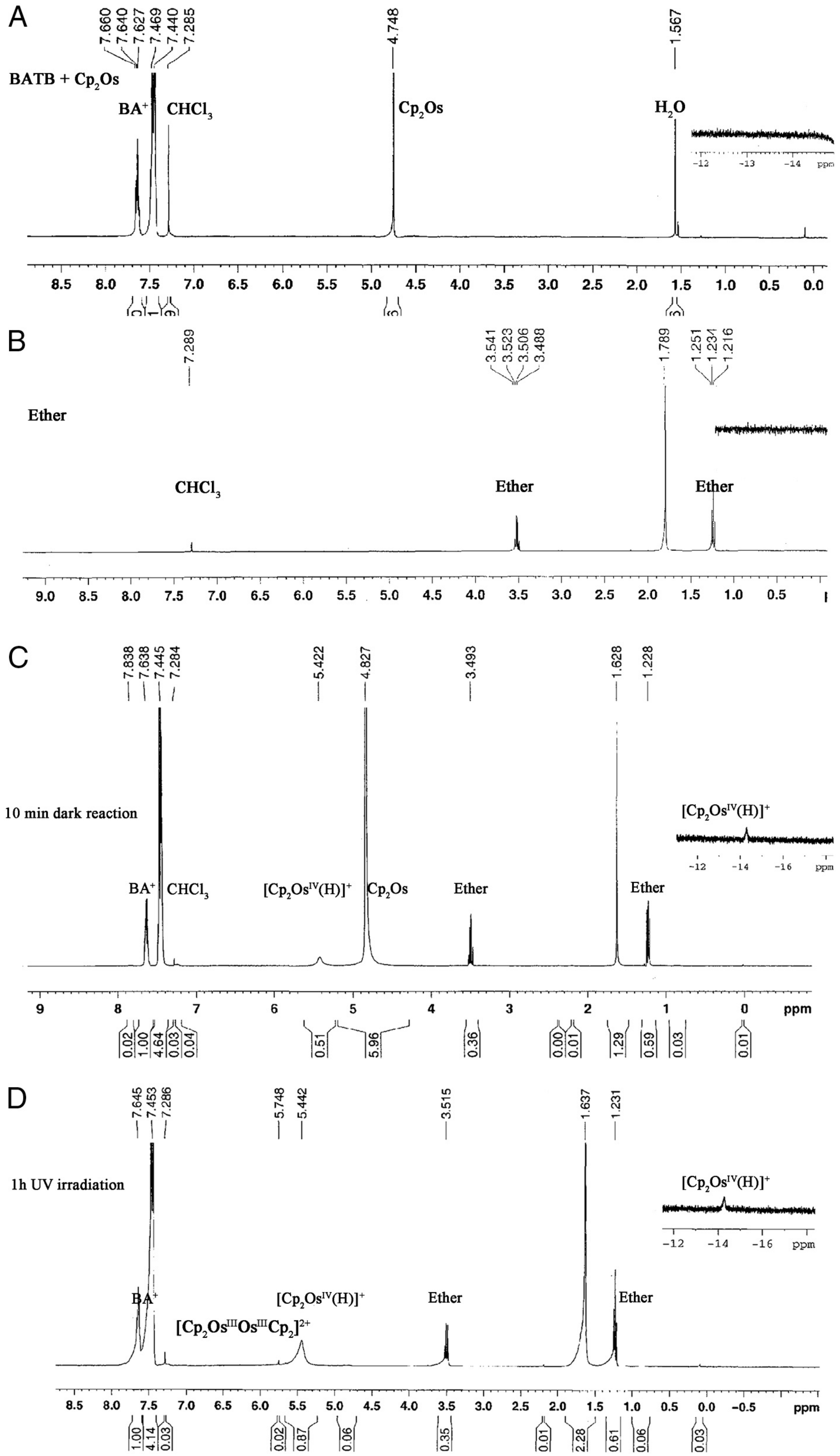

Fig. S2. (*A*) Proton nuclear magnetic resonance spectroscopy (^{1}H NMR) of the same amount of BATB and osmocene in deuterated chloroform (CDCl$_3$) phase; (*B*) ^{1}H NMR of CDCl$_3$ phase after mixing with 10 mM lithium tetrakis-(pentafluorophenyl)borate (LiTB) in aqueous phase for 30 min in dark in the absence of 0.1 M H_2SO_4; (*C*) ^{1}H NMR of 5 mM BATB and 10 mM osmocene in CDCl$_3$ phase after shaking with 10 mM LiTB in aqueous phase for 10 min in dark in the presence of 0.1 M H_2SO_4; and (*D*) ^{1}H NMR of the organic phase same treated in *C* and then irradiated with UV light for 1 h.

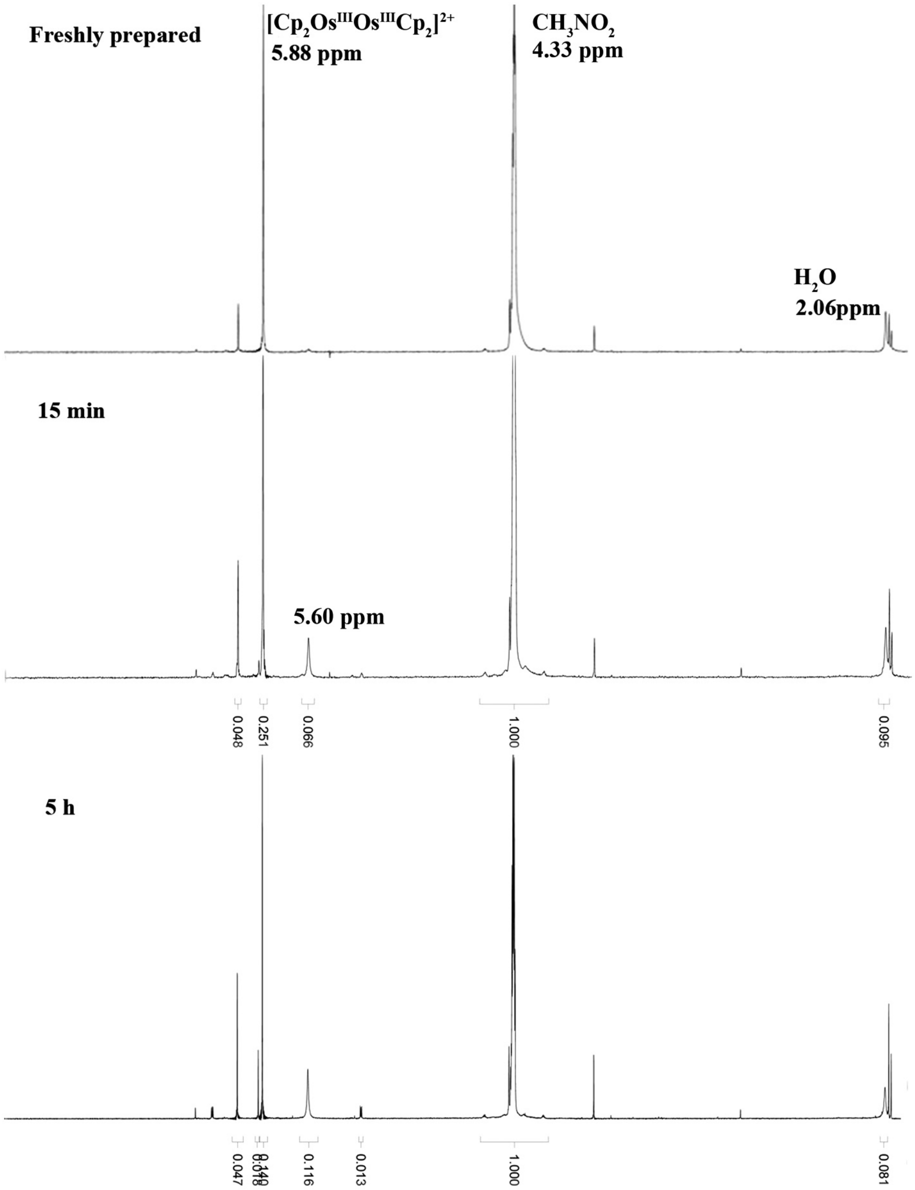

Fig. S3. ^1H NMR of $[Cp_2Os^{III}Os^{III}Cp_2]TB_2$ ($\delta = 5.88$ ppm) in deuterated nitromethane (CD_3NO_2) ($\delta = 4.33$ ppm) phase with time.

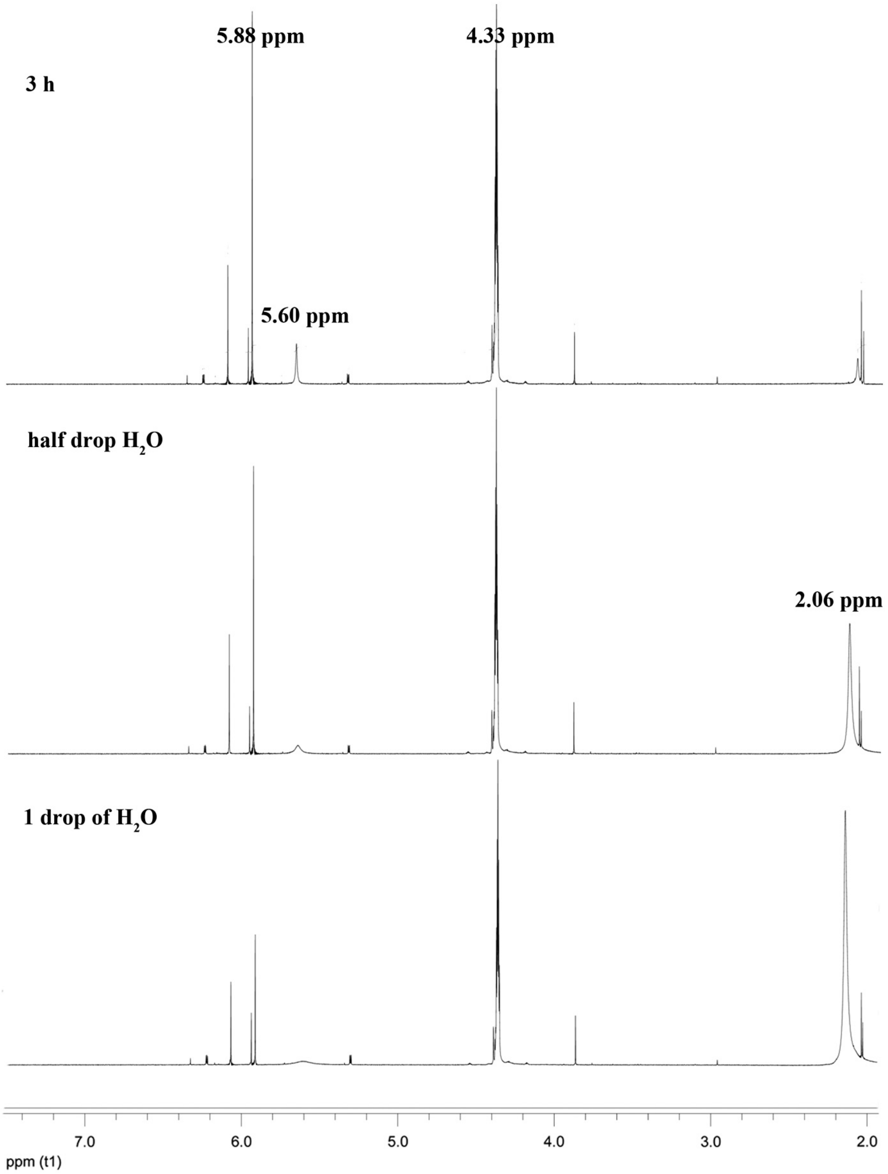

Fig. S4. ^1H NMR of $[Cp_2Os^{III}\text{-}Os^{III}Cp_2]TB_2$ in CD_3NO_2 phase for 3 h under anaerobic conditions and upon addition of half drop (*c.a.* 0.4 μL) and one drop (*c.a.* 0.5 μL) of H_2O ($\delta = 2.06$ ppm).

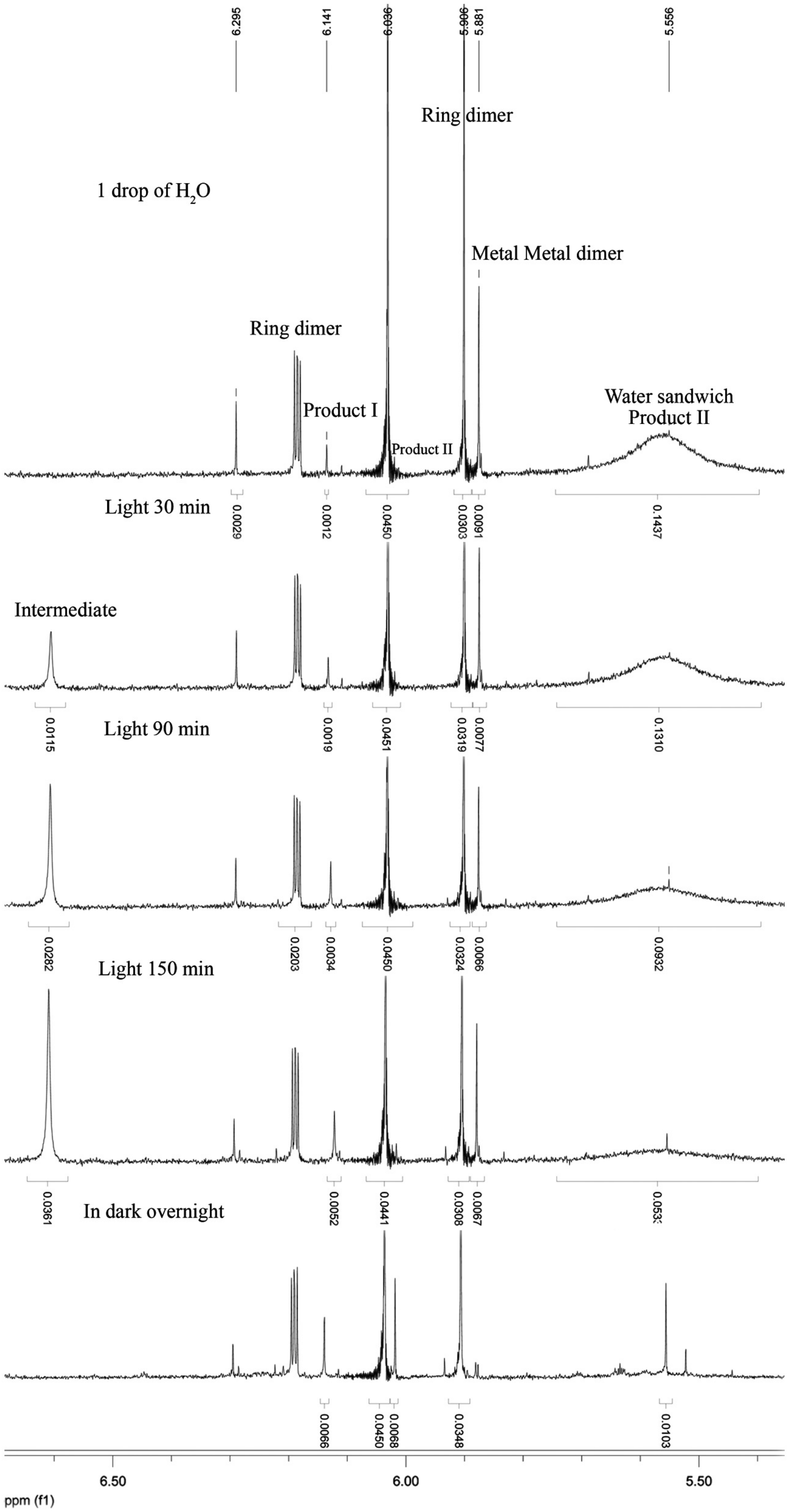

Fig. S5. ^{1}H NMR of $[Cp_2Os^{III}\text{-}Os^{III}Cp_2]TB_2$ in CD_3NO_2 phase on addition of water and upon irradiation of light.

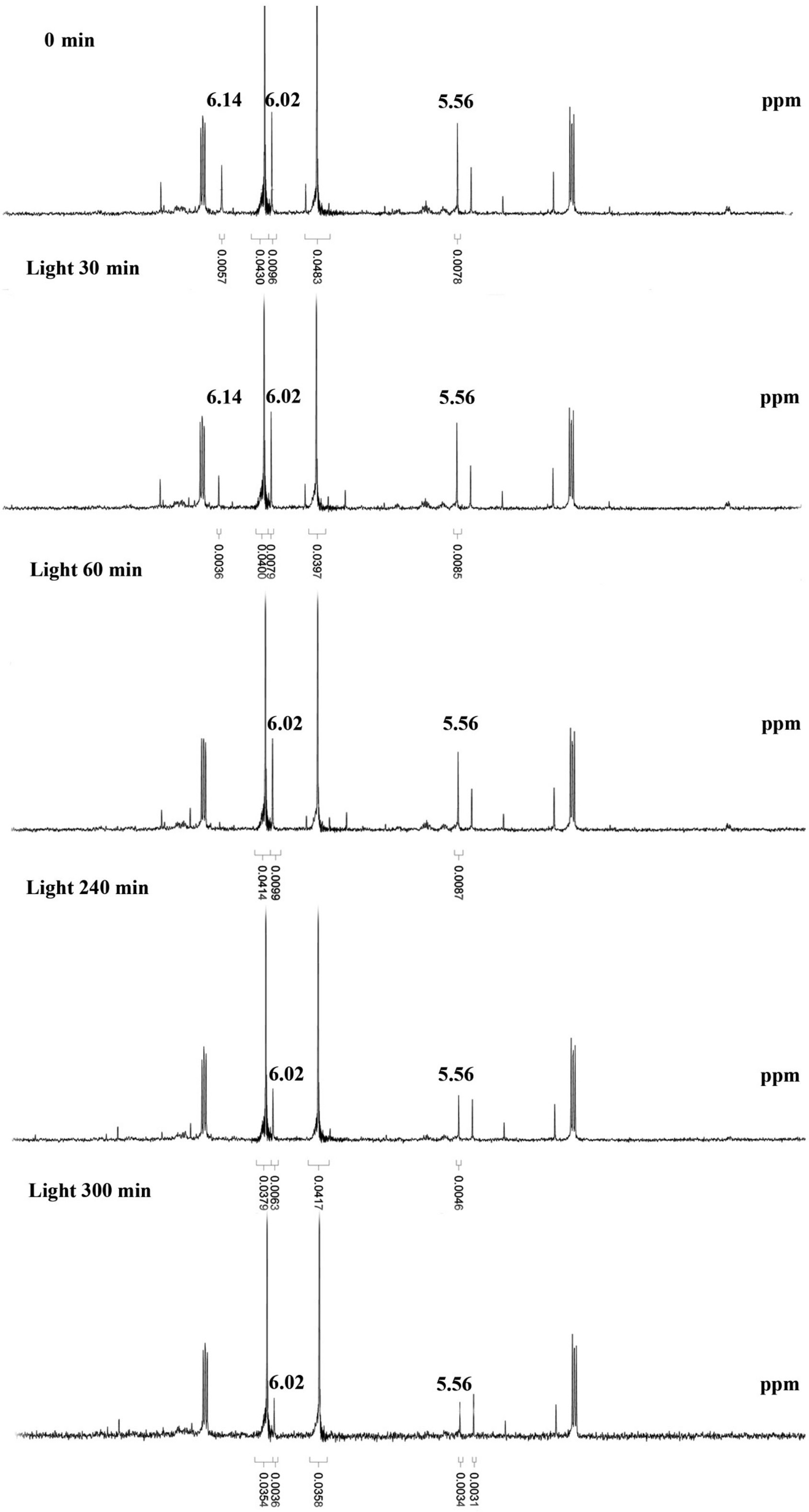

Fig. S6. ^{1}H NMR of products in Fig. S5 upon irradiation of white light.

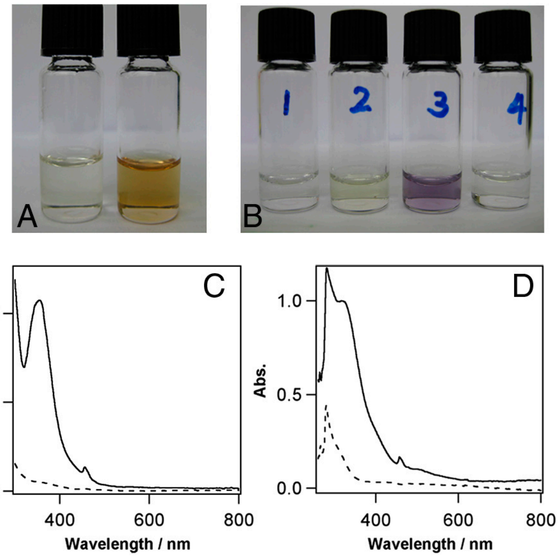

Fig. S7. (*A*) Photographic illustrations of the organic phase of the two-phase reactions controlled by tetrakis-(pentafluorophenyl)borate (TB^-) partition before (*Left*) and after (*Right*) reaction for 3 h. (*B*) Flask 1: water phase after 3 h of the two-phase reaction; flask 2: flask 1 + 0.1 M NaI; flask 3: flask 2 + starch; and flask 4: 5 mM LiTB + 0.1 M HCl + 0.1 M NaI + starch, (*C*) UV-visible spectra of the aqueous phase before (dotted line) and after (full line) treatment with 0.1 M NaI of the two-phase reaction. (*D*) UV-visible spectra of the DCE phase before (dotted line) and after (full line) shake flask experiments.

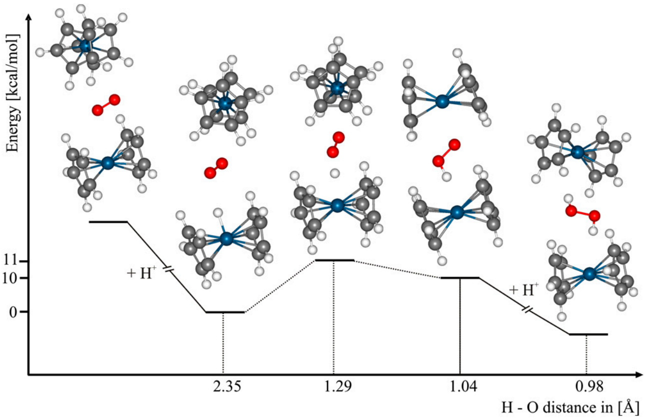

Fig. S8. Oxygen reduction mechanism by osmocene.

Table S1. Relative ΔH_{298} energies (in kcal/mol) for different dimerization reactions and reactions of water splitting computed at B3LYP-dDsC/cc-pVDZ, B3LYP/cc-pVDZ, and M06L/cc-pVDZ levels in the gas phase and in 1,2-DCE solvent

	B3LYP-dDsC	B3LYP		M06L	
Reaction no.	1,2-DCE	Gas	1,2-DCE	Gas	1,2-DCE
2	−16	47	−9	32	−18
5	23	7	2	24	17
7	3	−10	−4	2	5
13	−13	37	−13	34	−13
8	−4	−54	−7	−50	−2
10	16	23	0	39	14
11	1	−64	−10	−48	4
12	13	33	4	37	9

See the main text for numbered reactions.